International Institute for
Applied Systems Analysis
IIASA www.iiasa.ac.at

Real-Time Forecasting of Air Pollution Episodes in the Venetian Region. Part I: The Advection-Diffusion Model. Part II: The Kalman Predictor

Runca, E., Melli, P., Spirito, A., Fronza, G. and Tonielli, A.

IIASA Research Report
December 1979

REAL-TIME FORECASTING OF AIR POLLUTION EPISODES IN THE VENETIAN REGION

Part I: The Advection–Diffusion Model
E. Runca, P. Melli, and A. Spirito

Part II: The Kalman Predictor
G. Fronza, A. Spirito, and A. Tonielli

RR-79-11
December 1979

INTERNATIONAL INSTITUTE FOR APPLIED SYSTEMS ANALYSIS
Laxenburg, Austria

Research Reports, which record research conducted at IIASA, are independently reviewed before publication. However, the views and opinions they express are not necessarily those of the Institute or the National Member Organizations that support it.

SUMMARY

Most mathematical representations of air pollution phenomena consist of nondynamic relationships between average pollutant concentrations, emission rates of the sources, and a few meteorological variables such as atmospheric stability class, and wind speed and direction. These mathematical models (Gaussian) are generally adequate to simulate long-term average concentrations (e.g. yearly or seasonal) and are therefore useful when the allocation and design of pollutant sources must be decided. In most cases, however, the allocation and design of the stacks are only one side of the air quality management problem. In particular meteorological and/or emission situations, even an optimally planned system of sources may give pollutant levels well above admissible standards. These high pollution events, called episodes, have rapid dynamics (at hourly time scales or less) and in most cases cannot be adequately described by Gaussian models.

In principle, the most suitable representation of episodes should be obtained by integrating the advection–diffusion equation, which gives an accurate description (both in time and space) of the dispersion of a pollutant. Unfortunately, the input of the advection–diffusion model consists of extremely detailed information about meteorology and emission. In practical situations such detailed information is not available as the model inputs are affected by strong uncertainties. This situation explains why advection–diffusion models seldom perform satisfactorily, in particular when used for real-time prediction of future concentration levels at each time step on the basis of current information about concentrations, meteorology and emission.

In the present work, a different approach to the real-time forecasting problem is considered. It basically consists of embedding a

numerical solution scheme of the advection–diffusion equation into a stochastic framework and subsequently applying the well-known Kalman prediction techniques. Part I describes the numerical scheme as well as its application to the dispersion of sulphur dioxide in the Venetian lagoon area. Part II first shows that the numerical solution scheme illustrated in Part I can be interpreted as a discrete dynamical system which is subsequently turned into a stochastic system by introducing properly defined noise terms. Then, an adaptive Kalman predictor derived from the stochastic system is described, together with its real-time forecast performance for the Venetian case. In particular, the relevant four-hour-ahead forecast improvement with respect to the "deterministic" predictor, illustrated in Part I, is pointed out. The Kalman predictor will be introduced into a real-time control scheme of the industrial emissions in the Venetian area.

PREFACE

This report describes the research carried out in 1978 under the Resources and Environment Area (subtask on air pollution modeling and control). The object of the overall research, which has an expected duration of two years, is to set up a scheme for predicting ground-level pollutant concentrations for real-time control purposes (i.e., the action to be taken at the emission sources in the presence of forthcoming high pollution events). The forecasting scheme is described, together with its application to sulphur dioxide pollution in the Venetian lagoon area. The scheme is based on a complex mathematical model to be run on a computer and receiving at the beginning of each interval of time all the information (about the meteorological and emission situation) required for the prediction. The type of control action which should be taken on the basis of such a forecast is the object of the 1979 part of the research.

CONTENTS

Part I: The Advection–Diffusion Model

E. Runca, P. Melli, and A. Spirito

1 INTRODUCTION

By assuming that the gradient transfer theory holds for atmospheric turbulent diffusion processes, and also that the hypotheses of nondivergent airflow and molecular diffusion are negligible in comparison with turbulent (eddy) diffusion, it is possible to write the continuity equation for an air pollutant in the following form (three-dimensional advection–diffusion model):

$$\frac{\partial c}{\partial t} + \nabla \cdot vc = \nabla \cdot (\mathbf{K} \cdot \nabla c) + S + R \tag{1}$$

where c and v are pollutant concentration and wind field, respectively, $\mathbf{K}$ is the eddy diffusivity tensor, S is the source term, and R is the removal term.

Specifically, c and v in eq. (1) are averages over a time interval which is large in comparison with the dominant time scale of turbulent fluctuations but small in comparison with the time scale of variations of mean concentration and wind speed.

From eq. (1) and under simplifying assumptions (steady emission rate, no temporal or spatial variations in the wind field and atmospheric stability, no upper level inversion, no deposition of pollutant or chemical reaction between the pollutant and other substances), Sutton (1953) obtained the steady-state concentration downwind from a point source (Gaussian plume model). Since then, this formula has been extended to many multisource dispersion cases. Because of their simplicity, Gaussian models are largely used in applications, and in fact generally give reliable simulations of long term average concentrations (see for instance Pooler 1961, Calder 1971, Martin 1971, Runca *et al.* 1976).

Of course, when the assumptions listed above are no longer valid,

Gaussian models yield an unsatisfactory performance. This is particularly true for significant rapid increases and subsequent decreases of pollutant concentrations (episodes) owing to significant rapid variations in emission and/or meteorology. In these cases the only reliable approach is to solve eq. (1) by means of a numerical scheme. In the air pollution literature, there are few applications of numerical solution schemes of eq. (1) to real cases characterized by complex meteorological and emission conditions.

The first implementation of a numerical model in a multisource real case was due to Randerson (1970), who integrated eq. (1) by means of an explicit finite-difference scheme, in order to describe the dispersion of sulphur dioxide over the urban area of Nashville, Tennessee. The main restriction of Randerson's model was grid uniformity in the vertical direction. This caused computational problems and subsequently led to too great a limitation (60 m) on the height of the integration region.

A vertically expanding integration mesh (see also Bankoff and Hanzevack 1975) was used in the model developed by Shir and Shieh (1974), who simulated sulphur dioxide dispersion over St. Louis, Missouri. However, since they analyzed pollution due to urban emissions (which were nearly uniformly spread in the region), they used a grid uniformly spaced in the horizontal plane, and totalling 16,800 grid points.

The situation is quite different in the case described here, and concerns air pollution in the Venetian lagoon area due to the industrial emissions of Porto Marghera. As pointed out in detail in Section 3, the pollutant sources are concentrated in a relatively small region. Hence, it makes sense (for computational savings) to look for a numerical scheme that allows the use of a grid not uniformly spaced in the horizontal plane (see also Sardei and Runca 1976): specifically, a grid that expands on approaching zones farther and farther from the sources.

A numerical scheme that allows a nonuniform grid in all directions is described in Section 2, while the result of its application to the Venetian case is illustrated in Section 3. The description of pollution episodes was not satisfactory, mainly because of model input uncertainties. Hence, it was necessary to apply stochastic embedding and Kalman forecast techniques to the model (see Part II). Of course, the efficiency of the numerical scheme described above has made it possible to keep the computational burden of the Kalman predictor within reasonable limits.

Finally, it must be recalled that, in addition to the relatively small number of implementations of advection–diffusion models in real air

pollution cases, there is a conspicuous number of "theoretical" contributions that develop alternative numerical schemes for eq. (1). Some of these will be mentioned in the next section in the discussion of the accuracy, computational effort, and stability characteristics of the proposed algorithm.

2 THE PROPOSED NUMERICAL SCHEME

It is well-known that conventional finite difference schemes cannot describe accurately the advection term of eq. (1). In fact, they do not move air particles along the wind trajectories (i.e., the travel distance per time step is not equal to the mesh spacing), thus producing an artificial numerical "diffusion" both downwind and upwind. This "diffusion" can be of the same order of magnitude as the computed quantity (see for instance Robert and Weiss 1966).

Several methods have been proposed to overcome this drawback: the algorithm by Egan and Mahoney (1972) that involves the use of the first three momenta of the concentration distribution in each grid element; the mixed Eulerian–Lagrangian schemes like the "particle-in-cell" method (Sklarew *et al.* 1971, Lange 1973); and the procedure used by Runca and Sardei (1975). More recently, some papers (see for instance Melli 1976, Christensen and Prahm 1976) have shown the possibility of using Galerkin techniques in the treatment of the advection and diffusion of an air pollutant.

All these methods exhibit some unsatisfactory features – e.g., severe stability constraints, difficulty of treating boundary conditions, computer programming complexity. These drawbacks are largely avoided by the scheme described below which allows a non-uniform grid in all directions, requires a reasonable amount of computer time (see Section 3), is simple to be programmed and gives satisfactory accuracy. The scheme is a fractional step algorithm (see for instance Yanenko 1971) which integrates the advection terms via Carlson's method and the diffusion terms via Crank–Nicolson's procedure.

For simplicity, the illustration of the scheme is carried out on a

particular two-dimensional single-source form of eq. (1). However, extension to the three-dimensional multisource case, which was the one actually considered in the study on pollution in the Venetian lagoon, is straightforward (see Section 3).

The two-dimensional single-source form of eq. (1) is

$$\frac{\partial c}{\partial t} + v(z)\frac{\partial c}{\partial x} = \frac{\partial}{\partial z}\left[K^z(z)\frac{\partial c}{\partial z}\right] + Q\delta(z-h)\delta x \tag{2}$$

with initial and boundary conditions

$$c(x, z, 0) = 0 \tag{3}$$

$$c(x_w, z, t) = c(x_E, z, t) = 0 \qquad \forall z, \forall t \tag{4}$$

$$K^z\frac{\partial c}{\partial z} = 0 \qquad z = 0, H \qquad \forall x, \forall t \tag{5}$$

where h is the source height, H is the height of the inversion layer base, $v(z)$ is the wind speed (blowing in the x-direction) at level z, $K^z(z)$ is the vertical diffusion coefficient at level z, x_w is the abscissa of the western boundary of the integration region (just west of the source), x_E is the abscissa of the eastern boundary, Q is the source emission rate, and $\delta(.)$ is Dirac's function.

In eqs. (2)–(5), input (source and wind speed) and parameter (diffusion coefficient) dependence upon time have been neglected in order to simplify the notation in the description of the solution algorithm.

According to the method of fractional steps, eq. (2) is first split into three differential equations which respectively take into account the contributions of source, advection and diffusion terms:

$$\frac{\partial c}{\partial t} = Q\delta(z-h)\delta(x) \tag{6}$$

$$\frac{\partial c}{\partial t} + v(z)\frac{\partial c}{\partial x} = 0 \tag{7}$$

$$\frac{\partial c}{\partial t} = \frac{\partial}{\partial z}\left[K^z(z)\frac{\partial c}{\partial z}\right] \tag{8}$$

We now introduce the grid notation where Δx_i is the grid spacing between points (i, m) and $(i+1, m)$, and Δz_m is the grid spacing between (i, m) and $(i, m+1)$. Index i takes values $0, 1, \ldots, I+1$, and in particular $(1, mh)$ coincides with the source. Time is denoted by the index k; specifically, $c^k_{i,m}$ will represent the concentration at time $k\Delta t$ at point (i, m).

The index m takes values $0, 1, \ldots, M+1$; in particular, ground level and mixing layer height correspond to $m = 1$ and $m = M$, respectively. Moreover, $m = 0$ and $m = M + 1$ represent fictitious layers, which allow the satisfaction of boundary condition (5) by setting $\Delta z_0 = \Delta z_1$, $\Delta z_{M-1} = \Delta z_M$, $K_0^z = K_1^z$, $K_{M-1}^z = K_M^z$, $c_{i,0}^k = c_{i,1}^k$, $c_{i,M}^k = c_{i,M+1}^k$, $\forall k$, $\forall i$. Then consider the following algorithm for integrating eqs. (6)–(8) in the kth time interval.

(a) Contribution of the source term (solution of eq. (6)). Solving eq. (6) simply consists of adding the contribution of the source to the concentration field at time $k\Delta t$. The precise step is given by

$$c_{1,mh}^* = c_{1,mh}^k + \frac{4Q\Delta t}{(\Delta x_1 + \Delta x_0)(\Delta z_{mh} + \Delta z_{mh-1})}$$

$$c_{i,m}^* = c_{i,m}^k \quad \text{for} \quad (i,m) \neq (1,mh)$$

where $c_{i,m}^*$ denotes the concentration field after the step.

(b) Contribution of the advection term (solution of eq. (7)). First consider the forward time, backward space, finite difference approximation to eq. (7):

$$c_{i,m}^{**} = c_{i,m}^* - (v_m \Delta t/\Delta x_i)(c_{i,m}^* - c_{i-1,m}^*) \tag{9}$$

where $c_{i,m}^{**}$ is the concentration field after the step. Scheme (9) has first order accuracy and the Courant condition for numerical stability requires that

$$v_m \Delta t < \Delta x_i \tag{10}$$

To a first order approximation, eq. (9) can be written

$$\frac{\partial c}{\partial t} + v_m \frac{\partial c}{\partial x} = \frac{v_m}{2}(\Delta x_i - v_m \Delta t)\frac{\partial^2 c}{\partial x^2}$$

After many time steps, the numerical errors associated with eq. (9) can be quantified by the pseudodiffusion coefficient

$$P = (v_m/2)(\Delta x_i - v_m \Delta t)$$

which reduces to zero for

$$v_m \Delta t = \Delta x_i \tag{11}$$

Since the wind is a function of the vertical coordinate, namely v_m is not constant with m, in view of eq. (10), condition (11) can be satisfied only at the height where the wind speed is a maximum. In contrast, P

should obviously be zero, at least at source height ($m = mh$) where the highest concentration gradients occur.

A solution to this problem has been provided by Carlson (see for instance Richtmyer and Norton 1967). His scheme is illustrated in Figure 1 in the (x, t) plane (m = constant), where the broken trajectories I and II correspond to situations $v_m \Delta t < \Delta x_i$ and $v_m \Delta t \geqslant \Delta x_i$, respectively. Specifically, according to Carlson's scheme, if situation II of Figure 1 occurs, eq. (9) can be replaced by

$$c^{**}_{i,m} = c^{*}_{i-1,m} - (\Delta x_i / v_m \Delta t)(c^{**}_{i-1,m} - c^{*}_{i-1,m}) \tag{12}$$

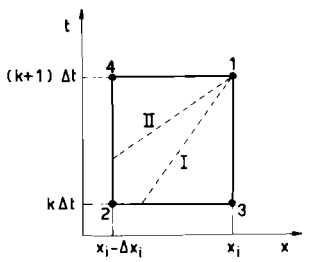

FIGURE 1 Carlson's scheme in the (x, t) plane: I is the trajectory for $v_m \Delta t < \Delta x_i$; II is the trajectory for $v_m \Delta t \geqslant \Delta x_i$.

The use of eq. (12) instead of eq. (9) for $v_m \Delta t \geqslant \Delta x_i$ makes Carlson's scheme unconditionally stable and allows a reduction of the truncation error to zero at source height by choosing $\Delta x_1 = v_{mh} \Delta t$.

(c) Contribution of the diffusion term (solution of eq. (8)). A numerical approximation to eq. (8) can be obtained by the method of Crank and Nicolson (1947):

$$c^{k+1}_{i,m} = c^{**}_{i,m} + \tfrac{1}{2} \{D_z[c^{k+1}_{i,m}] + D_z[c^{**}_{i,m}]\} \tag{13}$$

where

$$D_z[c^{k+1}_{i,m}] = (\Delta t / \Delta z^2_m)[K^z_{m+1} c^{k+1}_{i,m+1} - (K^z_{m+1} + K^z_{m-1}) c^{k+1}_{i,m} + K^z_{m-1} c^{k+1}_{i,m-1}]$$

is the standard difference operator for centered diffusion and c^{k+1} denotes the concentration field at time $(k + 1)\Delta t$.

The overall algorithm is here summed up for commodity:

$$c^{*}_{1,mh} = c^{k}_{1,mh} + \frac{4Q\Delta t}{(\Delta x_1 + \Delta x_0)(\Delta z_{mh} + \Delta z_{mh-1})} \tag{14'}$$

$$c^{*}_{i,m} = c^{k}_{i,m} \quad \text{for} \quad (i,m) \neq (1,mh) \tag{14''}$$

$$c^{**}_{i,m} = \begin{cases} c^{*}_{i,m} - (v_m \Delta t/\Delta x_i)(c^{*}_{i,m} - c^{*}_{i-1,m}) & v_m \Delta t < \Delta x_i \\ c^{*}_{i-1,m} - (\Delta x_i/v_m \Delta t)(c^{**}_{i-1,m} - c^{*}_{i-1,m}) & v_m \Delta t \geqslant \Delta x_i \end{cases} \tag{15'}$$

(15'')

$$c^{k+1}_{i,m} = c^{**}_{i,m} + \tfrac{1}{2}\{D_z[c^{k+1}_{i,m}] + D_z[c^{**}_{i,m}]\} \tag{16}$$

Though algorithm (14)–(16) is first order, it is more accurate than other, more complex, first and second order schemes. This better performance depends not only on the possibility of having zero truncation error at source height, but also on the method of fractional steps itself. This clearly arises from the following considerations.

Assume for simplicity a uniform grid ($\Delta x_i = \Delta x$, $\Delta z_m = \Delta z$). Then, by eliminating the intermediate fields c^{*} and c^{**}, eqs. (14)–(16) yield, for $v_m \Delta t = \Delta x$,

$$c^{k+1}_{i,m} = c^{k}_{i-1,m} + \frac{1}{2}\left\{D_z[c^{k+1}_{i,m}] + D_z\left[c^{k}_{i-1,m} + \frac{Q\Delta t}{\Delta x \Delta z}\right]\right\} + \frac{Q\Delta t}{\Delta x \Delta z} \tag{17}$$

The corresponding approximation to eq. (2) by the direct scheme (i.e., the scheme obtained by using the same finite difference operator but without splitting) is

$$c^{k+1}_{i,m} = c^{k}_{i-1,m} + \frac{1}{2}\left\{D_z[c^{k+1}_{i,m}] + D_z[c^{k}_{i,m}]\right\} + \frac{Q\Delta t}{\Delta x \Delta z} \tag{18}$$

By comparing eqs. (17) and (18), the following conclusions can be drawn.

(i) After k time intervals, while the fractional step scheme moves the pollutant front up to $v_m k\Delta t$, the direct scheme has a time lag of Δt, i.e., moves the front up to $v_m(k-1)\Delta t$.

(ii) In the region $x > 0$, where no source exists, eq. (18) approximates the diffusion operator along x = constant, while eq. (17) approximates it along the trajectory segment $\Delta x = v_m \Delta t$. By choosing $\Delta x = v_{mh}\Delta t$, eq. (17) holds at source height so that transport as well as diffusion are properly described in the region of maximum concentration gradients.

(iii) The fractional step scheme computes the new concentration values by exploiting the three "most relevant" points of the mesh, namely (see Figure 1) points 1, 2, 3 or 1, 2, 4 (depending

on whether the trajectory through point 1 precisely intersects Δx or Δt).

As a further comment, it must be pointed out that the suitability of Carlson's scheme to the advection step derives from the fact that in the region with the largest concentration gradients, in view of the choice $\Delta x_1 = v_{mh}\Delta t$, the Courant number is close to unity. Hence all Fourier modes are transported with a velocity close to wind speed and with negligible dissipation. Far from this region, where the concentration field gets smoother, only low frequency harmonics are required for its representation. For such harmonics, even if the Courant number is small, dispersion and dissipation errors are limited (Stone and Brian 1963, Robert and Weiss 1966).

Finally, it must be recalled that there are other fractional step procedures illustrated in the air pollution literature (see for instance Shir and Shieh 1974, Bankoff and Hanzevack 1975). The basic difference between such schemes and algorithm (14)–(16) is that they treat only the vertical terms with an implicit formulation, while the remaining steps are solved via an explicit approach. Hence the horizontal grid spacing, limited by stability conditions, is uniform, and subsequently the computational effort is higher. As pointed out in the Introduction, the choice is justified by the uniform distribution of the sources (domestic sources instead of the industrial sources considered in the present study).

Apart from obvious computational savings, a non-uniform grid in the horizontal plane allows the exact location of grid points in monitoring stations, thus avoiding any interpolation when comparing forecast and observed data.

3 APPLICATION OF THE FORECASTING SCHEME TO THE VENETIAN CASE

3.1 DESCRIPTION OF THE AREA AND POLLUTION PROBLEM

The area under consideration (Figure 2) is located in the northeastern part of Italy, at the upper shore of the Adriatic Sea. It includes part of the extreme end of the Padana Plain and part of the Venetian lagoon; precisely it consists of the urban centers of Mestre, Marghera and Venice and the industrial area of Porto Marghera (one of the largest in Europe). The urban centers of Mestre and Marghera, situated on the mainland, have

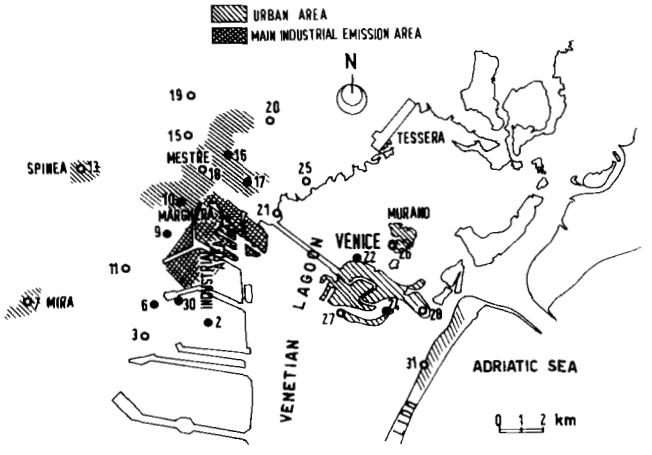

FIGURE 2 Venetian lagoon area and monitoring network: ●, station working since February 1973; ○, station working since February 1974.

developed very rapidly in the last three decades and now have a surface area of about 10 km^2. The industrial area is about 20 km^2 and its main activities include oil refining, petrochemical production, metallurgical processing of iron and other metals, and electric power production. Six kilometers from the mainland, in the middle of the Lagoon, is the historical center of Venice, covering an area of 6 km^2 and standing on a cluster of small islands.

The air pollution problem in the region has already been analyzed in a number of studies, e.g., the influence of meteorological factors on pollution levels has been investigated by Zannetti *et al.* (1977). Moreover, mathematical models, both deterministic (Runca *et al.* 1976) and "black box" stochastic (Finzi *et al.* 1977, Finzi *et al.* 1979), have been used for simulating or predicting long-term or short-term average SO_2 concentrations in the area.

In particular, Zannetti *et al.* (1977) analyzed the occurrence of episodes both in the historical center of Venice and in the mainland. It turned out that most of the pollution episodes occur in the industrial area, while the few concerning Venice correspond to winter winds blowing from the industrial area and are lower in intensity. Hence, using concentration measurements in the historical center would not add much information to a control scheme of air quality. Thus the present model has been implemented only in correspondence with the region shown in Figure 2. Of course, this choice has significantly reduced the computational effort.

3.2 INPUT DATA SET

Data concerning each of the 74 industrial sources (distributed in the Industrial Area shown in Figure 2) were obtained directly from 1971 National Census figures. An idea of the overall emission in the region can be obtained from the estimated pollutant released from industry, totalling 160,000 tons per year, in addition to approximately 10,000 tons per year from domestic heating. The location and average SO_2 emission rate of each source were available. Plume rises have been computed through the CONCAWE formula.

Both the meteorological and the concentration data used in the present study were provided by the monitoring network (Figure 2) installed by Tecneco on behalf of the Governmental Department of Health. This network consists of one meteorological station and 24 SO_2-monitoring sensors.

The meteorological station, 15 m above the ground, records hourly

wind speed and direction, temperature, pressure, humidity, rainfall, cloudiness, and fog. Wind direction is recorded according to the eight sectors of the compass, thus introducing an indetermination of ± 22° 30′.

Concentration data recorded by the 24 monitoring sensors are transmitted to a small computer which elaborates the data and records the hourly average values as well as daily statistics. In 1973, the year to which this study refers, only ten stations were in operation. Two of these are located in Venice; the remainder are the stations considered in this application.

In general terms, concentration data exhibit satisfactory reliability, although this is not true for the other types of data. In fact, emission data are only average rates, a very rough input when modeling an episode, partly or mainly due to extra-release. With respect to meteorological measurements, one station obviously cannot point out the spatial variation of wind and diffusion parameters. These input uncertainties alone are enough to explain the poor performance of the advection–diffusion model (see Section 3.4) and the subsequent reformulation in stochastic terms (Part II of the present work).

3.3 MODEL SPECIFICATIONS

The region of interest (16.5 km x 18.0 km) has been discretized by means of 10 x 12 x 7 grid points. The horizontal grid spacing ranges from a minimum of 1 km to a maximum of 2.5 km (see Figure 3, where the monitoring stations, all coincident with grid points, are also reported). The vertical grid sizes were specified as follows:

$$\Delta z_m = \begin{cases} 50\,\text{m} & m = 1, 2 \\ 75\,\text{m} & m = 3, 4 \\ (H - 250)/2 & m = 5, 6 \end{cases}$$

Since no measurement of the mixing depth H was available, H was kept at 500 m in all simulations.

On the above mesh, the following form of eq. (1) has been used (in contrast to eqs. (1) and (2), the input and parameter dependence upon time is explicitly pointed out):

$$\frac{\partial c}{\partial t} + v_x(z, s(t)) \frac{\partial c}{\partial x} + v_y(z, s(t)) \frac{\partial c}{\partial y}$$

$$= K^x(s(t)) \frac{\partial^2 c}{\partial x^2} + K^y(s(t)) \frac{\partial^2 c}{\partial y^2} + \frac{\partial}{\partial z}\left[K^z(z, s(t)) \frac{\partial c}{\partial z}\right] + S(x, y, z) \quad (19)$$

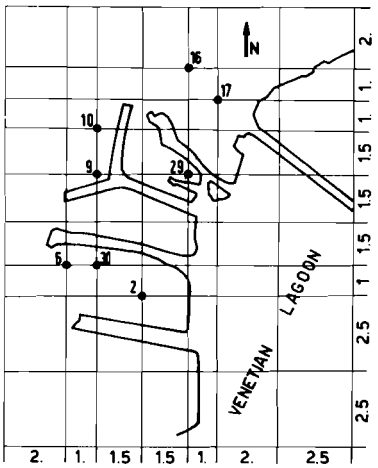

FIGURE 3 Geometry of the grid in the horizontal plane with distances in kilometers: •, stations working since February 1973, labeled in accordance with the Tecneco classification.

with initial and boundary conditions: $c(x, y, z, t) = 0$; $t = 0$, $K^z \partial c/\partial z = 0$, $z = 0, H$. At the side boundaries,

$$c(x, y, z, t) = 0 \qquad \forall t \tag{20}$$

In eq. (19), $S(x, y, z, t)$ is the source term, $v_x(z, s(t))$ and $v_y(z, s(t))$ are the wind speed components in the horizontal plane, and $s(t)$ denotes atmospheric stability at time t in accordance with the classification by Pasquill (1971). Specifically, Pasquill characterizes air turbulence by six classes ranging from A (strong instability) to F (extreme stability). The class has been determined for each time step from the wind and cloud data supplied by the meteorological station.

Boundary condition (20) is acceptable since the integration region is extended enough in the horizontal plane for pollution to be actually negligible at its boundaries. Clearly, from eq. (19), the wind field has only horizontal components, a standard assumption in advection–diffusion modeling (though questionable in an area characterized by sea breezes).

Moreover, as also shown in eq. (19), the wind field is considered to be uniform in each horizontal plane. Such a uniform field at level z has been evaluated using the power law

$$v_m(t) = v_R(t)\,(z_m/z_R)^{\alpha(s(t))} \tag{21}$$

where $v_m(t)$ is the wind vector at the mth level ($z = z_m$) at time t; $v_R(t)$ is

TABLE 1 Wind and diffusion parameters versus Pasquill stability classes.

$s(t)$	$\alpha(s(t))$	$\rho(s(t))$	$K^z(z_R, s(t))$ ($m^2\ s^{-1}$)	$K^x(s(t)) = K^y(s(t))$ ($m^2\ s^{-1}$)
A	0.05	6	45	250
B	0.1	6	15	100
C	0.2	4	6	30
D	0.3	4	2	10
E	0.4	2	0.4	3
F	0.5	2	0.2	1

the wind vector supplied at time t by the meteorological station (see Section 3.2), which is situated at z_R (15 m); and $\alpha(s(t))$ is the given function of stability reported in Table 1 (first column).

$K^z(z, s(t))$ is obtained by modifying the classic formula by Shir and Shieh (1974) in the following way:

$$K^z(z, s(t)) = K^D(s(t))z \exp[-\rho(s(t))z/H]$$

The values of $\rho(s(t))$ are reported in Table 1 (second column). $K^D(s(t))$ is obtained from

$$K^D(s(t)) = z_R^{-1} K^z(z_R, s(t)) \exp[\rho(s(t))z_R/H]$$

where $K^z(z_R, s(t))$ is the vertical diffusion coefficient at the level of the meteorological station and is reported in Table 1 (third column).

Finally, for the horizontal diffusion coefficients, it has been assumed that $K^x(s(t)) = K^y(s(t))$. These values are reported in Table 1 (fourth column).

3.4 SIMULATION RESULTS

The fractional step procedure (14)–(16), described in Section 2 for the two-dimensional eq. (2), has been applied to the three-dimensional advection–diffusion model (19) (the period considered was March–October, 1973). The extension of algorithm (14)–(16) to the solution of eq. (19) is straightforward and consists of a source step of the form of eq. (14), two advection steps of the form of eq. (15) in the x and y directions, respectively, and three diffusion steps of the form of eq. (16) in the x, y and z directions, respectively.

The comparison between simulation results and real data is favorable with respect to low or medium pollution periods but disappointing in the presence of episodes. For example, Figure 4 shows the dynamics of a

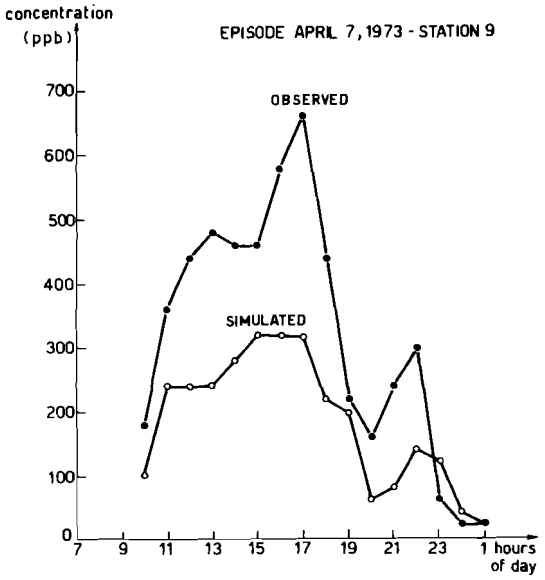

FIGURE 4 Simulation and measured values for an episode in station 9 on April 7, 1973.

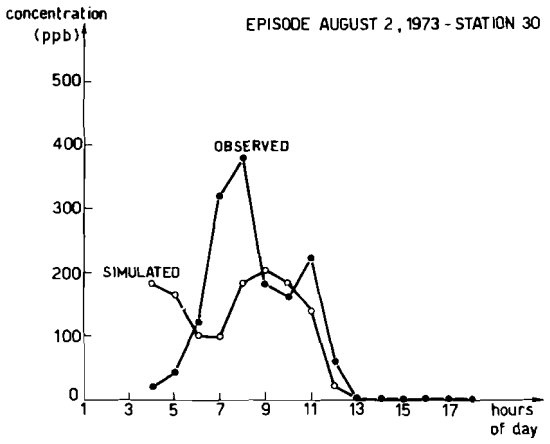

FIGURE 5 Simulation and measured values for an episode in station 30 on August 2, 1973.

relevant episode (peak more than twice the admissible standard) together with model simulation values. It is worthwhile adding that in practice the episode only affected the station (9) whose record is reported in Figure 4.

Other stations did not measure "extraordinary" pollution and there model fitting has been satisfactory. A similar result has been obtained for another relevant 1973 episode (Figure 5).

In both cases the discrepancies between model and reality can be reasonably ascribed to input uncertainty, due mainly to lack of information about extra-release by some polluter. Figures 4 and 5 prove the statement made in the Introduction that advection–diffusion models are accurate representations of the phenomenon but usually their input uncertainties do not allow an acceptable description of pollution episodes. Hence it is of no use to look for sophisticated numerical accurate solution algorithms; they can give only negligible improvement in addition to a possibly relevant enhancement of computation times. On the contrary, a significant step ahead has been achieved by embedding the model in a stochastic environment; this is illustrated in Part II.

4 REFERENCES

Bankoff, S.G., and E.L. Hanzevack (1975) The adaptive filtering transport model for prediction and control of pollutant concentration in an urban airshed. Atmospheric Environment **9**: 793–808.

Calder, K.L. (1971) A climatological model for multiple source urban air pollution. NATO/CCMS, Air Pollution **5**.

Christensen, O., and L.P. Prahm (1976) A pseudospectral model for dispersion of atmospheric pollutants. Journal of Applied Meteorology **15**: 1284–1294.

Crank, J., and P. Nicolson (1947) A practical method for the numerical solution of partial differential equations of the heat conduction type. Proceedings of the Cambridge Philosophical Society **43**.

Egan, B.A., and J.R. Mahoney (1972) Numerical modeling of advection and diffusion of urban area sources pollutants. Journal of Applied Meteorology **11**: 312–322.

Finzi, G., G. Fronza, S. Rinaldi, and P. Zannetti (1977) Modeling and forecast of the dosage population product in Venice. Proceedings of the IFAC Symposium on Environmental Systems, Planning, Design and Control, edited by H. Akashi and Y. Sawaragi. Oxford: Pergamon Press.

Finzi, G., P. Zannetti, G. Fronza and S. Rinaldi (1979) Real-time prediction of SO_2 concentration in the Venetian lagoon area. Atmospheric Environment **13**: 1249–1255.

Lange, R. (1973) ADPIC – A three-dimensional computer code for the study of pollutant dispersal and deposition under complex conditions. Report UCRL–51462. California: Lawrence Livermore Laboratory.

Martin, D.O. (1971) An urban diffusion model for estimating long term average values of air quality. Journal of the Air Pollution Control Association **21**: 16–19.

Melli, P. (1976) An application of the Galerkin method to the Eulerian–Lagrangian treatment of time-dependent advection and diffusion of air pollutants. Proceedings of the International Conference on Finite Elements for Water Resources, Princeton, New Jersey.

Pasquill, F. (1971) Atmospheric Diffusion. Princeton, New Jersey: Van Nostrand.

Pooler, F. (1961) A prediction model of mean urban pollution for use with standard wind roses. International Journal of Air and Water Pollution **4**: 199–211.

Randerson, D. (1970) A numerical experiment in simulating the transport of sulfur dioxide through the atmosphere. Atmospheric Environment **4**: 615–632.

Richtmyer, R.D., and K.W. Morton (1967) Difference Methods for Initial-Value Problems. New York: Interscience.

Robert, K.V., and N.O. Weiss (1966) Convective difference schemes. Mathematics of Computation **20**: 272–299.

Runca, E., and F. Sardei (1975) Numerical treatment for time-dependent advection and diffusion of air pollutants. Atmospheric Environment **9**: 69–80.

Runca, E., P. Melli, and P. Zannetti (1976) Computation of long-term average SO_2 concentrations in the Venetian area. Applied Mathematical Modeling. Environmental, Social and Engineering Systems **1**: 9–15.

Sardei, F., and E. Runca (1976) An efficient numerical scheme for solving time-dependent problems of air pollution advection and diffusion. Proceedings of the Seminar on Air Pollution Modeling, IBM Italy, Venice.

Shir, C.C., and L.J. Shieh (1974) A generalized urban air pollution model and its application to the study of SO_2 distributions in the St. Louis Metropolitan Area. Journal of Applied Meteorology **13**: 185–204.

Sklarew, R.C., A.J. Fabrick, and J.A. Prager (1971) A particle-in-cell method for the numerical solution of the atmospheric diffusion equation, and application to air pollution problems. Report 3SR-844, Systems, Science and Software, La Jolla, California.

Stone, H.L., and P.L.T. Brian (1963) Numerical solution of convective transport problems. American Institute of Chemical Engineers Journal **9**: 681–688.

Sutton, O.G. (1953) Micrometeorology. New York: McGraw-Hill.

Yanenko, N.N. (1971) The Method of Fractional Steps. Berlin: Springer-Verlag.

Zannetti, P., P. Melli, and E. Runca (1977) Meteorological factors affecting SO_2 pollution levels in Venice. Atmospheric Environment **11**: 605–616.

Zannetti, P., G. Finzi, G. Fronza, and S. Rinaldi (1977) Time series analysis of Venice air quality data. Proceedings of the IFAC Symposium on Environmental Systems, Planning, Design and Control, edited by H. Akashi and Y. Sawaragi. Oxford: Pergamon Press.

Part II: The Kalman Predictor

G. Fronza, A. Spirito, and A. Tonielli

1 INTRODUCTION

In the last ten years, stochastic mathematical models such as ARIMA (AutoRegressive Integrated Moving Average) or seasonal ARIMA have been used to fit time series of air pollutant concentrations (see, for instance, Merz *et al.* 1972, Chock *et al.* 1975, McCollister and Wilson 1975, Tiao *et al.* 1975). In an ARIMA-type representation, the concentrations (or related variables) at a certain instant are expressed as linear combinations of previous concentration values and random terms (noise), which are specified in a statistical sense (i.e., are properly described in terms of a random process). Thus, in ARIMA models the physical causes of the phenomenon (meteorological variables and emission rates of the sources) are not distinguished in the input, or, equivalently, the effect of the physical causes on pollutant concentrations is represented only by the random terms.

In accordance with the techniques recommended by Box and Jenkins (1970), ARIMA models can be used with real-time forecasting to predict future concentrations, at the beginning of each period, on the basis of previously recorded pollution levels. However, the absence of physical inputs means that ARIMA predictors are unable to give a satisfactory forecast performance in the presence of pollution episodes. In fact the rapid increases and subsequent decreases in concentrations can only be explained by pointing out the existence of a particular meteorological and/or emission situation.

Therefore, a better real-time episode predictor can be derived from the so-called ARIMAX stochastic mathematical representations (ARIMA with eXogenous inputs; see for instance Young and Whitehead 1977, and Box and Jenkins 1970). In such models, pollutant concentrations at a

certain instant are expressed as linear combinations of previous concentration values and a linear combination of present and previous physical inputs with noise terms (see for instance Finzi *et al.*, 1977a, 1977b, and 1978).

Because of their simplicity, ARIMAX models represent a serious alternative to the advection–diffusion models illustrated in Part I. A more detailed comparison of the two appoaches leads to the following conclusions.

(1) Advection–diffusion models give an adequate description of the phenomenon, but suffer from strong input uncertainties (see Part I). Moreover, the parameters (diffusion coefficients) have a direct physical meaning but their assignment relies upon sometimes questionable assumptions on meteorology (see Part I, Section 3.2). Finally, advection–diffusion models require complex numerical solution schemes. The overall result is usually an unsatisfactory episode forecast performance (see Part I, Section 3.4) requiring a relatively large amount of effort.

(2) Stochastic ARIMAX representations have an arbitrary (though, obviously, not unreasonable) structure, but this arbitrariness as well as input and parameter uncertainties are accounted for (in a statistical sense) by the model itself through the noise terms. Moreover, information on the noise statistics plays an important useful role in the real-time predictor derived from the stochastic model (it is the well-known Kalman predictor, see for instance Kalman 1960, and Jazwinski 1970; it should be noted that the forecast techniques recommended by Box and Jenkins 1970 for the ARIMAX and abovementioned models represent a particular case of the Kalman predictor). The result is usually an acceptable episode forecast performance (see for instance Finzi *et al.* 1977a and 1977b). Furthermore, the computational effort required, due to the implementation both of a technique for the estimation of model parameters (see for instance Kashyap and Rao 1976, parameters of ARIMAX have no direct physical sense and hence must be estimated from recorded time series) and of the Kalman predictor, is relatively slight.

The comparison, in terms of both episode forecast performance and effort, seems to be in favor of ARIMAX, although there is one more consideration. By their own nature, ARIMAX only have a sense if they are characterized by a few variables, i.e., if they give only an aggregate

description of the phenomenon. In fact, it is practically impossible to set up a reliable multivariate ARIMAX of many dimensions. In other terms, it is reasonable and feasible to fix an arbitrary model structure that gives an acceptable representation of the cause–effect mechanism "as a whole". However, it is not possible to establish *a priori* a model structure that describes the mechanism in detail (comparable with the detail of the results supplied by the numerical solutions of advection–diffusion equations). In conclusion, the comparison between the two approaches is partially improper, since advection–diffusion models aim to achieve a detailed description of the concentration field (usually with unsatisfactory forecast performance and a relatively large amount of effort) while ARIMAX give an aggregate picture (typically, with few spatial averages) of the pollution field (generally with acceptable performance and little effort).

The aim of Part II is to supply the advection–diffusion model with the attractive characteristics of stochastic representations, in order to obtain a detailed and precise real-time forecast of the pollution phenomenon. The formal procedure is illustrated in Section 2, where the numerical solution scheme developed in Part I is turned into a stochastic model (see also Desalu *et al.* 1974, Bankoff and Hanzevack 1975, and Sawaragi and Ikeda 1974). As in the case of ARIMAX, a Kalman predictor can be derived from such a stochastic model (Section 3), although here the structure of the predictor is not arbitrary and "aggregate" but has a physical basis (since it originates from the advection–diffusion equation) and is extremely detailed.

In fact, the four-hour-ahead episode forecast of the Kalman predictor is very satisfactory when applied to the Venetian lagoon pollution case (Section 4). In particular, the performance is conspicuously better than that of all previous predictors for the area (see Part I and Finzi *et al.* 1977).

2 TRANSFORMATION OF THE NUMERICAL SOLUTION SCHEME OF THE ADVECTION–DIFFUSION EQUATION INTO A STOCHASTIC DYNAMICAL SYSTEM

For simplicity, the procedure for turning the numerical solution scheme of the air pollutant advection–diffusion equation into a stochastic discrete dynamical system will be carried out on the single-source, two-dimensional form of the scheme, illustrated in detail in Section 2 of Part I. This algorithm is rewritten here by explicitly pointing out the dependence of input (source and wind speed) and parameters (diffusion coefficients) upon the time index k (this dependence was deleted for notational simplicity in Part I but is important for the purposes of this section).

$$c^*_{1,mh} = c^k_{1,mh} + \frac{4Q^k \Delta t}{(\Delta x_1 + \Delta x_0)(\Delta z_{mh} + \Delta z_{mh-1})} \tag{1'}$$

$$c^*_{i,m} = c^k_{i,m} \qquad (i, m) \neq (1, mh) \tag{1''}$$

$$c^{**}_{i,m} = \begin{cases} c^*_{i,m} - (v^k_m \Delta t/\Delta x_i)(c^*_{i,m} - c^*_{i-1,m}) & v^k_m \Delta t < \Delta x_i \quad (2') \\ c^*_{i-1,m} - (\Delta x_i/v^k_m \Delta t)(c^{**}_{i-1,m} - c^*_{i-1,m}) & v^k_m \Delta t \geqslant \Delta x_i \quad (2'') \end{cases}$$

$$c^{k+1}_{i,m} = c^{**}_{i,m} + \tfrac{1}{2}\{D^k_z[c^{k+1}_{i,m}] + D^k_z[c^{**}_{i,m}]\} \tag{3}$$

where

$$D^k_z[c^{k+1}_{i,m}] = (\Delta t/\Delta z^2_m)\{K^z_{m+1}(s(k))c^{k+1}_{i,m+1} - [K^z_{m+1}(s(k)) + K^z_{m-1}(s(k))]\, c^{k+1}_{i,m} + K^z_{m-1}(s(k))c^{k+1}_{i,m-1}\} \tag{4}$$

$s(k)$ denotes Pasquill's stability class for the kth time interval.

The procedure described in Sections 2.1 and 2.2 interprets eqs. (1)–(3) as a discrete dynamical system and then makes this system stochastic by adding "noise terms". In the following, the notation $|b^k_{i,m}|$

for $i = 0, 1, \ldots, I+1$; $m = 0, 1, \ldots, M+1$ will denote the row vector $|b^k(0,0) \quad b^k(1,0) \ldots b^k(I+1,0) \quad b^k(0,1) \ldots b^k(I+1, M+1)|^T$ (T = vector transposition symbol).

2.1 INTERPRETATION OF THE NUMERICAL SCHEME AS A DISCRETE DYNAMICAL SYSTEM

Let $X(k) = |c^k_{i,m}|$, $X^* = |c^*_{i,m}|$ and $E(k) = |e^k_{i,m}|$, where $e^k_{i,mh} = 4Q^k \Delta t/(\Delta x_1 + \Delta x_0)(\Delta z_{mh} + \Delta z_{mh-1})$, and $e^k_{i,m} = 0$ for $(i,m) \neq (1, mh)$. Then the source step (1) takes the compact form

$$X^* = X(k) + E(k) \tag{5}$$

For the advection step, we first define the Courant number:

$$\alpha^k_{i,m} = v^k_m \Delta t/\Delta x_i \tag{6}$$

It is then possible to rewrite eqs. (2′) and (2″) in the following forms:

$$c^{**}_{i,m} = c^*_{i,m} - \alpha^k_{i,m}(c^*_{i,m} - c^*_{i-1,m}) \qquad \alpha^k_{i,m} < 1 \tag{2′a}$$

$$\alpha^k_{i,m} c^{**}_{i,m} = (\alpha^k_{i,m} - 1)c^{**}_{i-1,m} + \alpha^k_{i,m} c^*_{i-1,m}, \qquad \alpha^k_{i,m} \geqslant 1 \tag{2″a}$$

Let $X^{**} = |c^{**}_{i,m}|$ denote the concentration field after the advection step and let $\alpha^k = |\alpha^k_{i,m}|$.

If the Courant number is less than unity for all (i,m), only eq. (2′a) is active. This equation is a linear dependence of X^{**}-components on X^*-components and hence can be given the compact form

$$X^{**} = F'(\alpha^k)X^* \tag{7}$$

where $F'(\alpha^k)$ is a suitable matrix, whose entries only depend on α^k. In contrast, if the Courant number is greater than unity for all (i,m), only eq. (2′b) is active. This equation is an implicit definition of X^{**}, which can be made explicit by expressing X^{**} as a function of the boundary conditions and of the field X^*. Equation (2″b) can also be interpreted as the state equation of a discrete dynamical system, where the space indexes (i,m) work as "time", X^{**} works as a state vector, X^* works as an input vector and the boundary conditions work as the initial conditions. Since system (2″b) is linear and since the boundary conditions are zero (see Part I), then

$$X^{**} = F''(\alpha^k)X^* \tag{8}$$

where $F''(\alpha^k)$ is a suitable matrix depending only on α^k.

In view of eqs. (7) and (8), in the general case when the Courant index is less than unity at some grid points and greater than unity elsewhere,

it is possible to write the advection step in the compact form

$$X^{**} = F(\alpha^k)X^* \tag{9}$$

where $F(\alpha^k)$ is a suitable matrix whose entries only depend on α^k. Moreover, by defining the wind field $v(k) = |v_m^k|$ and by recalling the expression (eq. (6)) for the Courant index, eq. (9) can also be given the form

$$X^{**} = A(v(k))X^* \tag{10}$$

where $A(v(k))$ is a suitable matrix, whose entries only depend on the wind field.

For the z-diffusion step, first let

$$\beta_m^-(s(k)) = K_m^z(s(k))\Delta t/\Delta z_m(\Delta z_m + \Delta z_{m+1})$$
$$\beta_m^+(s(k)) = K_{m+1}^z(s(k))\Delta t/\Delta z_{m+1}(\Delta z_m + \Delta z_{m+1})$$

Using cumbersome but straightforward computations, it is possible to verify that eqs. (3)–(4) are equivalent to

$$\begin{aligned} c_{i,m+1}^{k+1} = {} & [\beta_m^+(s(k))]^{-1}\{[1 + \beta_m^-(s(k)) + \beta_m^+(s(k))]\, c_{i,m}^{k+1} \\ & - \beta_m^-(s(k))c_{i,m-1}^{k+1} - \beta_m^+(s(k))c_{i,m+1}^{**} - [1 - \beta_m^-(s(k)) \\ & - \beta_m^+(s(k))]\, c_{i,m}^{**} - \beta_m^-(s(k))c_{i,m-1}^{**}\} \end{aligned} \tag{3a}$$

By applying the argument used for $c_{i,m}^{**}$ in eq. (2a) to the implicit definition (3a) of $c_{i,m}^{k+1}$, and by recalling the vertical boundary conditions, an explicit expression of the concentration field at time $k + 1$ is produced:

$$X(k + 1) = B(s(k))X^{**}$$

where $X(k + 1) = |c_{i,m}^{k+1}|$ and $B(s(k))$ is a suitable matrix depending only on the stability class.

Finally, by eliminating the intermediate fields X^* and X^{**} in eqs. (5), (10) and (11), the overall algorithm takes the compact form

$$X(k + 1) = \phi(v(k), s(k))X(k) + \phi(v(k), s(k))E(k) \tag{12}$$

where $\phi(v(k), s(k)) = B(s(k))A(v(k))$. Equation (12) can be considered as the state equation of a discrete dynamical system having a state $X(k)$, and inputs $E(k)$, $v(k)$ and $s(k)$.

Moreover, if $y(k)$ denotes the vector of concentration measurements at time k (taken at monitoring stations coincident with grid points), an output transformation of the discrete system can be defined as

$$y(k) = HX(k) \tag{13}$$

where H is a matrix whose elements are either 0 or 1.

2.2 TRANSFORMATION OF THE DISCRETE SYSTEM INTO A STOCHASTIC SYSTEM

Embedding the discrete system (12), (13) in a stochastic environment simply means summing the random terms in its two relationships in order to represent the "inaccuracies" of the model itself. Specifically, the stochastic version of system (12), (13) is given by

$$X(k+1) = \phi(v(k), s(k))X(k) + \phi(v(k), s(k))E(k) + n(k) \qquad (12')$$

$$y(k) = HX(k) + w(k) \qquad (13')$$

where $n(k)$ is a stochastic term ("process noise") which accounts for all the sources of disagreement between the model and the actual dynamics of the pollution phenomenon (e.g., for neglected physical inputs in the advection–diffusion equation such as rain or chemical reactions, for errors introduced by the assignment of parameter values, for errors due to the model structure or to numerical inaccuracies). Moreover, $w(k)$ is a stochastic term ("measurement noise") which accounts for errors in measurements.

The random processes $\{n(k)\}_k$ and $\{w(k)\}_k$ are commonly assumed to be zero-mean white noises, i.e., to have a correlation structure of the following type ($E(.)$ is an expectation operator):

$$E[n(k)n^T(k+\tau)] = \begin{cases} Q(k) & \tau = 0 \\ 0 & \tau \neq 0 \end{cases}$$

$$E[w(k)w^T(k+\tau)] = \begin{cases} R(k) & \tau = 0 \\ 0 & \tau \neq 0 \end{cases}$$

The problem of evaluating $Q(k)$ and $R(k)$ is discussed in the next section, which is devoted to the description of the Kalman predictor derived from eqs. (12') and (13').

3 REAL-TIME PREDICTOR

The stochastic model (12′), (13′) can be used for real-time pollution forecasting, namely for predicting future concentration levels at the beginning of each time interval, on the basis of current information about concentrations, emission and meteorology. Specifically, the recursive one-step ahead forecast algorithm (Kalman predictor), derived from model (12′), (13′), is given by (see for instance Jazwinski 1970):

$$\hat{X}(k|k) = \hat{X}(k|k-1) + G(k)[Y(k) - H\hat{X}(k|k-1)] \tag{14}$$

$$\hat{X}(k+1|k) = \phi(v(k), s(k))\hat{X}(k|k) + \phi(v(k), s(k))E(k) \tag{15}$$

where $\hat{X}(k+1|k)$ is a prediction of $X(k+1)$ made at time k, namely at the beginning of the kth time interval; and $\hat{X}(k|k)$ is a filtered state, namely an *a posteriori* (i.e. at time k) estimation of $X(k)$ on the basis of the newly available datum $y(k)$. Precisely this estimation is given by eq. (14) as a correction of the previous forecast $\hat{X}(k|k-1)$ and is introduced in eq. (15) instead of $\hat{X}(k|k-1)$ in order to give a better prediction of $X(k+1)$.

$$G(k) = P(k|k-1)H^T[HP(k|k-1)H^T + R(k)]^{-1} \quad \text{(Kalman gain)} \tag{16}$$

$P(k|k-1) = E[(\hat{X}(k|k-1) - X(k))(\hat{X}(k|k-1) - X(k))^T]$ is the forecast error covariance matrix.

In turn, this covariance matrix is recursively evaluated through the following equations:

$$P(k|k) = P(k|k-1)\{I - H^T[HP(k|k-1)H^T + R(k)]^{-1}HP(k|k-1)\} \tag{17}$$

$$P(k+1|k) = \phi(v(k), s(k))P(k|k)\phi^T(v(k), s(k)) + Q(k+1) \quad (18)$$

The r-step ahead prediction ($r = 2, 3, \ldots$) is obtained recursively from

$$\hat{X}(k+r|k) = \phi(v(k+r-1), s(k+r-1))\hat{X}(k+r-1|k) + \phi(v(k+r-1), s(k+r-1))E(k+r-1) \quad (19)$$

The actual implementation of the Kalman predictor (14)–(19) raises a number of conceptual and practical problems which are now discussed in detail.

3.1 ASSIGNMENT OF $Q(k)$ AND $R(k)$

The correction *a posteriori* of the previous forecast $\hat{X}(k|k-1)$ to $\hat{X}(k|k)$ (a better initial state for the new prediction step (15)) is made in eq. (14) by weighting the new datum $y(k)$ through the Kalman gain $G(k)$. In turn, this weight matrix depends, in view of eqs. (16)–(18), on the noise intensities $Q(k)$ and $R(k)$. In conclusion, at every forecast step the Kalman predictor corrects ("filters") the initial state of the step by taking into account the noise intensities. Obviously, $Q(k)$ and $R(k)$ must be regarded as input data to the filter (14), (16)–(19), i.e., must be evaluated before the filtering is made. In principle, $R(k)$ should result from an analysis of the accuracy of the measurement system, while $Q(k)$ should result from considerations of fitting between the numerical scheme and the real world.

This is not accomplished in practice. Rather, $Q(k)$ and $R(k)$ are usually estimated by recursive algorithms, based on *a posteriori* analysis at each time step of the performance of the predictor at earlier time steps.

In fact, there are other types of adaptive Kalman predictors, namely Kalman predictors supplied with a recursive algorithm for *a posteriori* estimation of $Q(k)$ and $R(k)$. Unfortunately, the most rigorous predictors (see for instance Mehra 1970) cannot be applied to the present case, because of the nonstationarity of system (12′), (13′), i.e., because the matrix $\phi(v(k), s(k))$ is not the same for every k.

Thus, in the application described in Section 4, a heuristic adaptive approach has been followed, which represents a slight generalization of a procedure by Jazwinski (1969).

3.2 TREATMENT OF EMISSION UNCERTAINTIES

The adaptive mechanisms mentioned above (noise intensities updated at each time step) are commonly too weak to allow a good forecast of

pollution episodes when these are due to conspicuous (but unknown to the predictor) emission enhancements. Usually, a more robust correction is obtained by introducing an additive term $p(k)$ in eq. (12′):

$$X(k+1) = \phi(v(k), s(k))X(k) + \phi(v(k), s(k))E(k) + p(k) + n(k) \tag{12″a}$$

with dynamics

$$p(k+1) = p(k) \tag{12″b}$$

This procedure is called state enlargement and the Kalman predictor derived from model (12″a), (12″b), (13′) is called extended (see for instance Jazwinski 1970). Though often effective (Bankoff and Hanzevack 1975), extended (adaptive) Kalman predictors require the dimension of the state of the stochastic system to be doubled (from eq. (12″a), $p(k)$ has the same dimension as $X(k)$) and correspondingly the computational burden is greatly increased.

Hence, a simpler and less expensive, though rougher and heuristic, recursive adjustment of emission inputs has been considered in the present work. This involves modifying eq. (12′) as follows:

$$X(k+1) = \phi(v(k), s(k))X(k) + \phi(v(k), s(k))\theta(k)E(k) + n(k) \tag{12‴}$$

The scalar $\theta(k)$ is defined as

$$\theta(k) = \sum_l \hat{x}_l(k|k) \Big/ \sum_l \hat{x}_l(k|k-1) \tag{20}$$

where $\hat{x}_l(k|k)$ and $\hat{x}_l(k|k-1)$ are the l components of $\hat{X}(k|k)$ and $\hat{X}(k|k-1)$, respectively, and the summations are made over all components.

From eq. (20), $\theta(k)$ is a ratio between the total "mass" of pollutant estimated *a posteriori* (namely, after the arrival of the new measurement vector $y(k)$) and the "mass" previously forecast. If the two "masses" do not coincide, then an emission variation, occurring between time $(k-1)$ and time k and not revealed to the predictor, is assumed and the emission for the subsequent step (prediction of $X(k+1)$ made at time k) is correspondingly modified.

3.3 COMPUTATIONAL EFFORT

From eqs. (14)–(19), the implementation of the Kalman predictor implies at each iteration step the manipulation of square matrices of order equal to the number of grid points. Although the numerical scheme

described in Part I admits non-uniform grid spacing, the order of such matrices may easily be one thousand, corresponding to an intolerable computational burden. In order to reduce this burden, the following procedure by Bankoff and Hanzevack has been used.

(1) A certain number of disconnected subregions of interest (subregions where episodes usually occur) are selected. If $\mathscr{R}_1, \mathscr{R}_2, \ldots, \mathscr{R}_D$ denote such subregions, let $X_d(k)$, $d = 1, 2, \ldots, D$, be the vector of components of $X(k)$ corresponding to the grid points of $\mathscr{R}_d$. ($X_d(k)$ may be a subvector of thirty components, say). For simplicity, assume initially that the ordering between the components of $X(k)$ is rearranged, so that $X(k)$ can be partitioned as

$$X(k) = |X_1^T(k)X_2^T(k)\ldots X_D^T(k) \vdots X_{\text{out}}^T(k)|^T$$

where $X_{\text{out}}(k)$ is the vector of $X(k)$ components corresponding to grid points out of any subregion.

(2) Apply the filter (14), (16)–(18) only to each subregion, namely evaluate the filtered subvectors $\hat{X}_1(k|k)$, $\hat{X}_2(k|k), \ldots, \hat{X}_D(k|k)$. Each of these D applications of the filtering procedure implies the manipulation of matrices of reasonable dimensions.

(3) Modify the forecast step (15) (and correspondingly (19)) by

$$\hat{X}(k+1|k) = \phi(v(k), s(k))\tilde{X}(k|k) + \phi(v(k), s(k))E(k) \quad (15')$$

where

$$\tilde{X}(k|k) = |\hat{X}_1^T(k|k)\hat{X}_2^T(k|k)\ldots\hat{X}_D^T(k|k)\hat{X}_{\text{out}}^T(k|k-1)|^T \quad (21)$$

From eqs. (15′) and (21) it turns out that procedure (1)–(3) simply corresponds to the filtering of a state subvector at each step of the Kalman predictor.

There is clearly a danger inherent in this method. As is apparent from eq. (21), the initial state $\tilde{X}(k|k)$ of the forecast step (15′) may turn out to be a very "irregular" concentration field, since only some of the state components have been filtered. In particular, strong variations may result between the components corresponding to subregion boundaries and those corresponding to grid points immediately outside the boundaries. Hence, "artificial" high gradients may be introduced, that have negative effects on the forecast step (15′) (which is only a step of the numerical scheme, described in part I, with initial field $\tilde{X}(k|k)$). Whether the distortion caused by partial filtering is relevant or not, it can be ascertained only by simulation of the Kalman predictor for the real case (see Section 4).

3.4 METEOROLOGICAL INPUT TO THE PREDICTOR

From eqs. (15) and (19), the forecast of r-step ahead concentration fields, made at the beginning of the kth time interval, requires a knowledge of emission, wind field and stability inputs for the time intervals $[k\Delta t, (k+1)\Delta t], [(k+1)\Delta t, (k+2)\Delta t], \ldots, [(k+r-1)\Delta t, (k+r)\Delta t]$.

The necessary information about emission in these future periods should in principle be available, since emission is a decision variable of polluters, who are assumed to collaborate or to be forced to collaborate with the prediction (if wrong information is supplied, the forecast quality is safeguarded by the correction mechanism described in Section 3.2).

However, future meteorology is obviously not known. There are basically two possible approaches to determine the wind and stability inputs required by the concentration predictor.

(1) Set up a meteorological predictor, whose forecasts are introduced as inputs into eqs. (15) and (19).
(2) Simply postulate a persistent meteorology (future wind and stability will be the same as those at present).

Clearly, the forecast performance of the concentration predictor under approach (2) is a lower bound, since it corresponds to the least accurate treatment of the meteorological inputs. However, the upper bound for such a performance corresponds to a situation where wind and stability inputs are supplied to eqs. (15) and (19) by a perfect meteorological predictor (with forecast values of wind and stability always equal to their future time values).

Moreover, the performance under approach (1) is expected to lie within the two bounds, its distance to the upper bound obviously depending on the quality of the meteorological forecast.

The above analysis about the sensitivity of concentration prediction to the treatment of meteorological inputs has actually been done in the Venetian lagoon study and is illustrated in detail in Section 4.

4 THE APPLICATION OF THE PREDICTOR TO THE VENETIAN LAGOON STUDY

The Venetian lagoon air pollution problem and monitoring network have already been described in Part I (Section 3), together with the three-dimensional model (eq. (19) of Part I) used in the application.

Of course, a "stochastic embedding" procedure, quite similar to the one illustrated in Section 2, holds for the numerical solution scheme of the three-dimensional advection–diffusion equation. The resulting stochastic model is rewritten here by pointing out that wind speed has two (horizontal) components in this case:

$$X(k+1) = \phi(v(k), d(k), s(k))X(k) + \phi(v(k), d(k), s(k))E(k) + n(k) \quad (22)$$

$$y(k) = HX(k) + w(k) \quad (23)$$

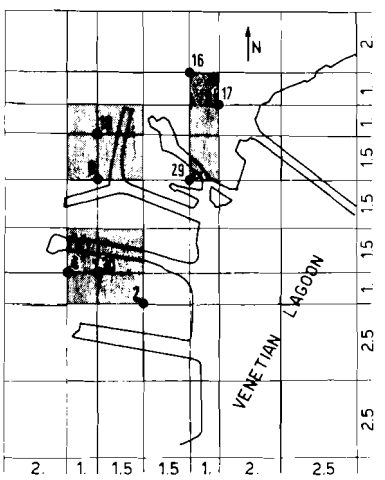

FIGURE 1 Ground level of the discretization grid (distances in kilometers) with stations (•) and subregions (shaded areas).

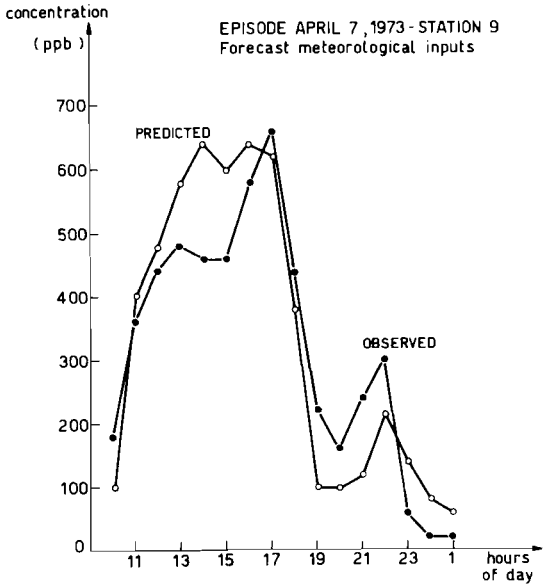
concentration
(ppb)
EPISODE APRIL 7 , 1973 - STATION 9
Forecast meteorological inputs
PREDICTED
OBSERVED
700
600
500
400
300
200
100
0
11
13
15
17
19
21
23
1
hours
of day

a

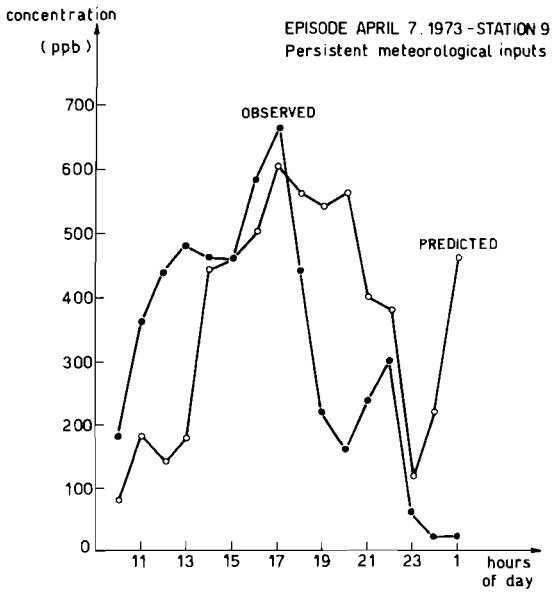
concentration
(ppb)
EPISODE APRIL 7. 1973 - STATION 9
Persistent meteorological inputs
OBSERVED
PREDICTED
700
600
500
400
300
200
100
0
11
13
15
17
19
21
23
1
hours
of day

b

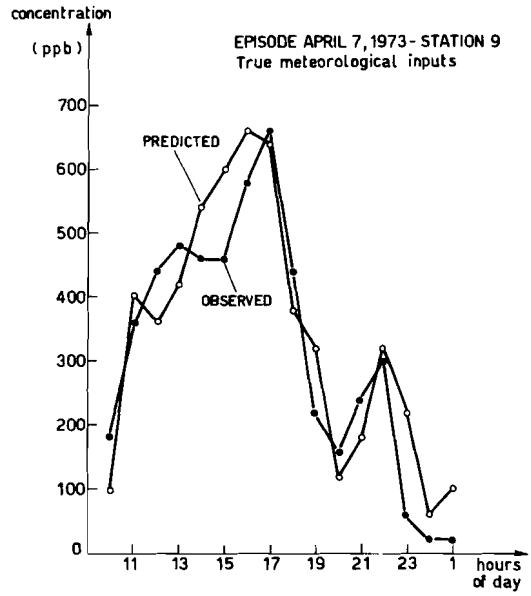

c

FIGURE 2 Four-hour-ahead episode Kalman prediction with: (a) forecast; (b) persistent; (c) true meteorological inputs (April 7, 1973, station 9).

where $v(k)$ and $d(k)$ denote the vector of wind intensities at different levels, and the wind direction, respectively. For the Kalman predictor derived from system (22), (23), the specifications concerning Sections 3.3 and 3.4 must be supplied.

The locations of the three grid subregions mentioned in Section 3.3 (subregions where the concentration field is filtered) are illustrated in Fig. 1. The shaded areas of Fig. 1 represent the bases of the three subregions at ground level ($m = 1$) and correspond to the most polluted zones. On the vertical axis, each subregion reaches the level $m = 3$, namely has an extension of two layers above the ground. The three subregions correspond to 18, 18 and 16 state variables, respectively.

Concerning Section 3.4, the Kalman predictor of future concentrations was run in correspondence with three different types of meteorological inputs.

(a) Inputs given by a mathematical meteorological predictor. Precisely, for $f = 1, 2, \ldots, r - 1$, a forecast $\hat{s}(k + f|k)$ (made at time k

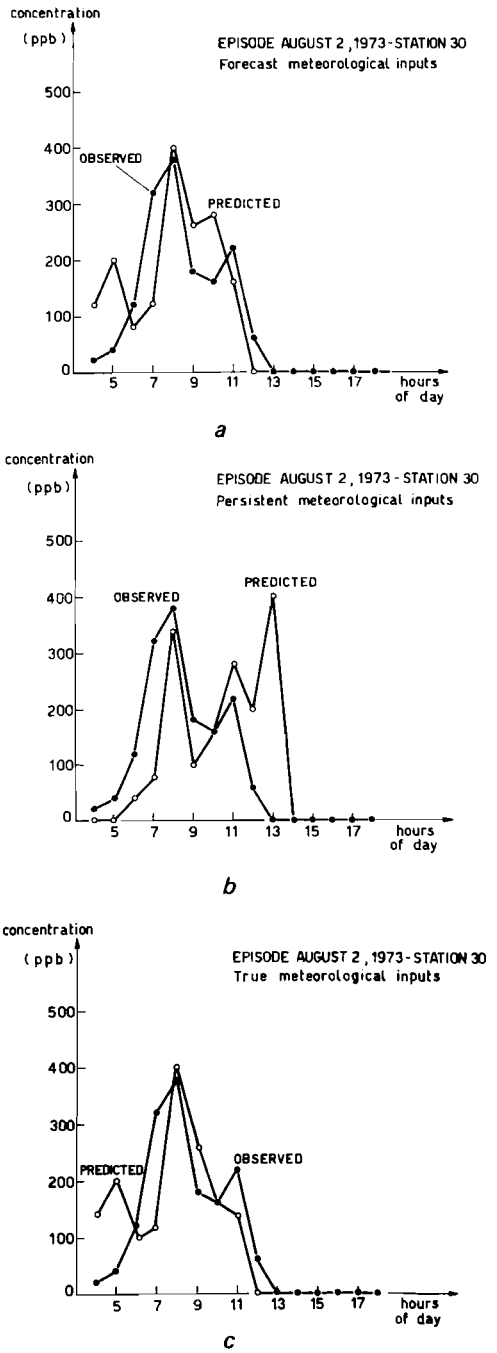

FIGURE 3 Four-hour-ahead episode Kalman prediction with: (a) forecast; (b) persistent; (c) true meteorological inputs (August 2, 1973, station 30).

for the stability class at time $k+f$) was obtained in accordance with the following simple probabilistic criterion:

$$\hat{s}(k+f|k) \rightarrow \max_{s(k+f)} \Pr\{s(k+f)|s(k-1), q\}$$

where $\Pr\{s(k+f)|s(k-1),q\}$ is the probability of having class $s(k+f)$ at time $k+f$, given the information that the class is $s(k-1)$ in the interval $[(k-1)\Delta t, k\Delta t]$ and that time $k\Delta t$ is the qth hour of the day ($q = 1, 2, \ldots, 24$).

Similarly, the wind direction sector was forecast in accordance with the criterion

$$\hat{d}(k+f|k) \rightarrow \max_{d(k+f)} \Pr\{d(k+f)|d(k-1), q\}$$

Finally, wind intensity in the meteorological station was forecast by means of an ARIMA predictor (see Box and Jenkins 1970). From this forecast, predictions $\hat{v}(k+f|k)$ of the whole future profiles of wind intensities were obtained through the power law already illustrated in Part I, Section 3.

(b) Inputs given by assuming a persistent meteorology ($v(k+f) = v(k-1), d(k+f) = d(k-1), s(k+f) = s(k-1)$).

(c) Inputs given by assuming a perfect meteorological predictor, i.e. true inputs.

The four-hour-ahead forecast performance under the three input conditions is shown in Fig. 2 for the episode of April 7, 1973, and in Fig. 3 for the episode of August 2, 1973. As expected, approach (a) gives a performance intermediate between (b) and (c), but very close to the ideal situation (c). In fact the correlations between forecast and true concentration data were 0.90, 0.32, 0.92 (Figs. 2(a)–(c), respectively) and 0.76, 0.50 and 0.77 (Figs. 3(a)–(c), respectively). It is clear from a comparison of Figs. 2 and 3 with the corresponding performance of the numerical scheme alone (Figs. 4 and 5 of Part I) that the quality has improved.

For the remainder of the concentration field, it must first be recalled that the above-mentioned episodes are characterized by a strongly non-uniform field: to be precise, by a relevant peak in one station (station 9 for the episode of April 7, 1973, and station 30 for the episode of August 2, 1973) and by relatively low concentrations elsewhere. Such low concentrations are satisfactorily forecast by the Kalman predictor, namely the "artificial gradient effect" (caused by subregion filtering and mentioned in Section 3.3) has not occurred. However, there has been a certain overestimation of the field outside the station affected by the pollution

peak. This is due to the correction mechanism for the emissions, illustrated in Section 3.2, which is based on the multiplicative scalar coefficient $\theta(k)$, and hence results in the simultaneous enhancement of all the emissions. Thus the existence of an episode around a station forces the correction mechanism to increase all emissions and subsequently to raise all the forecast fields. Of course this effect could be avoided by setting up a suitable selective mechanism for correction of the emissions.

In nonepisode situations, the predictor also gives good performance, but this is not a particularly significant result. Finally, for computational times, each four-hour-ahead forecast required approximately three minutes on an IBM 370 computer.

5 REFERENCES

Bankoff, S.G., and E.L. Hanzevack (1975) The adaptive filtering transport model for prediction and control of pollutant concentration in an urban airshed. Atmospheric Environment **9**: 793–808.

Box, G.E.P., and G.M. Jenkins (1970) Time series analysis, forecasting and control. San Francisco: Holden-Day.

Chock, D.P., T.R. Terrel, and S.B. Levitt (1975) Time series analysis of Riverside, California air quality data. Atmospheric Environment **9**: 978–989.

Desalu, A.A., L.A. Gould, and F.C. Schweppe (1974) Dynamic estimation of air pollution. IEEE Trans. on Automatic Control, **AC-19**: 904–910.

Finzi, G., G. Fronza, S. Rinaldi, and P. Zannetti (1977) Modeling and forecast of the dosage population product in Venice. Proceedings of the IFAC Symposium on Environmental Systems, Planning, Design and Control, edited by H. Akeshi and Y. Sawaragi. Oxford: Pergamon Press.

Finzi, G., G. Fronza, and A. Spirito (1977b) Univariate stochastic models and real-time predictors of daily SO_2 pollution in Milan. Proceedings of the NATO-CCMS 7th International Technical Meeting on Air Pollution Modeling, Louvain-la-Neuve, Belgium.

Finzi, G., G. Fronza, and S. Rinaldi (1978) Stochastic modeling and forecast of the dosage product. Atmospheric Environment **12**: 831–838.

Jazwinski, A.H. (1969) Adaptive filtering. Automatica: 475–495.

Jazwinski, A.H. (1970) Stochastic processes and filtering theory. New York: Academic Press.

Kalman, R.E. (1960) A new approach to linear filtering and prediction theory. Trans. of the ASME, Section D., Journal of Basic Engineering **82**: 17–25.

Kashyap, R.L., and A.R. Rao (1976) Dynamic stochastic models from empirical data. New York: Academic Press.

McCollister, G.M., and J.R. Wilson (1975) Linear stochastic models for forecasting daily maxima and hourly concentrations of air pollutants. Atmospheric Environment **9**: 417–423.

Mehra, R.K. (1970) On the identification of variances and adaptive Kalman filtering. IEEE Trans. on Automatic Control **AC-15**: 175–184.

Merz, P.H., L.J. Painter, and P.R. Ryason (1972) Aerometric data analysis–time series analysis and forecast of an atmospheric smog diagram. Atmospheric Environment **6**: 319–342.

Sawaragi, Y., and S. Ikeda (eds.) (1974) Proceedings of the Symposium on Modeling of the control and prediction of air pollution. Kyoto, Japan.

Tiao, G.C., G.E. Box, and W.J. Hamming (1975) A statistical analysis of the Los Angeles ambient carbon monoxide data 1955–1972. Journal of the Air Pollution Control Association **25**: 1129–1136.

Young, P. and P. Whitehead (1977) A recursive approach to time series analysis for multivariable systems. International Journal of Control **25**: 457–468.

RELATED IIASA PUBLICATIONS

RR-73-16	Subjective Probability Forecasting in the Real World: Some Experimental Results, by R.L. Winkler, A.H. Murphy.	$4.00, AS60
RR-77-5	Air Pollution Dispersion Models as used in Poland in Regional Development Planning, by J. Pruchnicki. MICROFICHE ONLY.	$3.00, AS45
RR-78-9	The Smeared Concentration Approximation Method: A Simplified Air Pollution Dispersion Methodology for Regional Analysis, by R.L. Dennis.	$7.00, AS100
RM-75-22	An Adaptive Identification and Prediction Algorithm for the Real-Time Forecasting of Hydrologic Time Series, by A. Szöllösi-Nagy.	$3.00, AS45
RM-75-26	A Reduced Dimensionality Method for the Steady-State Kalman Filter, by J. Casti.	$3.00, AS45
RM-75-64	Credibility Theory and Kalman Filtering with Extensions, by R.K. Mehra.	$3.00, AS45
RM-76-9	Application of the Kalman Filter to Cyclone Forecasting: 1. Methodology; 2. Typhoon Forecasting, by K. Takeuchi.	$5.00, AS70
RM-76-22	Regional Air Pollution Impact: A Dispersion Methodology Developed and Applied to Energy Systems, by R.L. Dennis. MICROFICHE ONLY.	$3.00, AS45

RM-76-44	Use of Kalman Filtering Techniques when the Parameters of a Regression Relationship are Changing over Time According to a Multivariate ARIMA Process, by J. Ledolter.	$3.00, AS45
RM-76-62	Application of the Kalman Filter to Cyclone Forecasting: 3. Hurricane Forecasting; 4. Additional Typhoon Forecasting, by K. Takeuchi.	$5.00, AS70

ORDERING INFORMATION

Orders for Publications should be sent to the Publications Department, International Institute for Applied Systems Analysis, A–2361 Laxenburg, Austria (tel. 02236/7521, ext. 401). Orders should include the publication number and should be accompanied either by a check payable to the IIASA Publications Department or by evidence of a bank transfer to: Creditanstalt Bankverein, Schottengasse 6, 1010 Vienna, Austria, Account No. 23–76788.

IIASA publications may also be purchased from the National Technical Information Service. Please contact NTIS at the following address for order and price information: NTIS, 5285 Port Royal Road, Springfield, VA 22161, USA.